A heliostat based on a three degree-of-freedom parallel manipulator

R.B. Ashith Shyam, Mohit Acharya, A. Ghosal*

Mechanical Engineering, Indian Institute of Science, Bangalore, India

ARTICLE INFO

ABSTRACT

In this paper, we propose a three-degree-of-freedom spatial parallel manipulator to track the sun in central receiver tower based concentrated solar power systems. The proposed parallel manipulator consists of three 'legs' each containing a passive rotary(R) joint, an actuated sliding or prismatic (P) joint and a passive spherical (S) joint and is known in literature as the 3-RPS manipulator. In contrast to existing serial mechanisms with two degrees-of-freedom, firstly it is shown that the extra actuator and enhanced mobility helps in reducing spillage losses and astigmatic aberration. Secondly, due to the three points of support, the beam pointing errors are less for wind and gravity loading or, alternately, the weight of the supporting structure to maintain desired deflections of the mirrors are significantly lower. Finally, the linear actuators used in the parallel manipulator do not require the use of large, accurate and expensive speed reducers. In this paper, we model the 3-RPS manipulator and derive the kinematics equations which give the motion of the linear actuators required to track the sun and reflect the incident solar energy at a stationary target at any time of the day, at any day of the year and at any location on the surface of the Earth. Finite element analysis is used to determine an optimized design which can reduce the weight of the supporting structure by as much as 60% as compared to the existing tracking mechanisms. A proportional, integral plus derivative (PID) control strategy using a low-cost processor is devised and a detailed simulation study is carried out to show that the proposed parallel manipulator performs better compared to the current tracking algorithms. Finally, a prototype of the parallel manipulator is manufactured and it is demonstrated that it is capable of performing autonomous sun tracking with the above mentioned advantages.

1. Introduction

The use of spatial parallel mechanisms have been gaining widespread acceptance in application specific purposes like camera orientation, scanning spherically shaped objects, beam aiming etc. (see, for example, (Dunlop and Jones, 1999; Li et al., 2006; Gosselin and Caron, 1999; Carricato and Parenti-Castelli, 2004; Ruggiu, 2010)). Recently, Cammarata (2015) has shown that by employing a large workspace two-degree-of-freedom (DOF) parallel manipulator for orienting photovoltaic (PV) panels, there can be an increase in electrical energy production by more than 17%. Altuzarra et al. (2014) proposed a complicated four degree-of-freedom parallel manipulator where the collector initially is kept (before the tracking starts) high above the ground and by letting it fall, under gravity, in a controlled manner using four sliders attached to it, the required orientation is achieved. This mechanism casts its own shadow on the collector and although, simulation results seem to be good, no prototype has been made and tested. Google Inc. (2017a,b) developed a novel method, using electric cable

drives, for changing the position and orientation of the reflector (mirror). Although they claim that this method would reduce the power consumption for tracking, the size and cost of the actuator system, their light weight frame design is susceptible to wind gusts and could be used only at places where wind velocities are very low.

In a central receiver (CR) system, the mirrors reflect the incident sun rays onto a stationary receiver tower throughout the day. The receiver tower may be several meters (70–195 m) high and the mirrors could be as far as 1.40 km away from the tower. The motion of the moving mirrors or heliostats are programmable and also calibrated periodically to ensure that the incident rays are always reflected to the receiver tower for all instants of time during a day and throughout a year. The receiver has a heat absorbing medium, like molten salts or steam, to absorb the thermal energy and this thermal energy is converted to electricity to satisfy the load – a storage enables CR systems to produce electricity even after dark and an installation named Crescent Dunes has 10 h of dispatchable storage (Mendelsohn et al., 2012). Due to the large number of heliostats reflecting the sun's energy to the receiver,

---

Nomenclature

γ	angle which the X axis of the $\{B\}$ makes with the East direction	C_d	coefficient of drag
		FoS	factor of safety
$\overrightarrow{GS}$	Sun vector	r_b	radius of the base equilateral triangle
ψ	Heliostat's angular location with respect to the local East direction	R_d	heliostat radial distance from the tower
		r_p	radius of the platform equilateral triangle
ρ	density of air	CR	Central Receiver
$\{B\}$	base co-ordinate system	DOF	Degree of Freedom
$\{M\}$	mirror co-ordinate system	OX-OY-OZ	Global co-ordinate system pointing to local East-local North and Zenith, respectively

---

the temperature achieved can be very high (565 °C at Ivanpah, USA (NREL, 2017))) and thus a higher efficiency is achieved in conversion to electrical energy when compared to photo-voltaic (PV) systems (Roman et al., 2006). In the existing CR systems, the mirrors are mounted as end-effector of a serial manipulator and essentially supported at the center. Due to such an arrangement, the deflection of the heliostats in presence of wind gusts may go beyond the acceptable beam error limit of 2–3 mrad (Vant-Hull, 2012). To minimize such degradation of solar image on the receiver aperture, a heavy backing or support structure needs to be provided.

The sun moves roughly in a East-West direction in a day and in a North-South direction with the seasons. Hence, two angles are involved and a two-DOF mechanism is required to track the sun. There are several serial arrangements and corresponding tracking algorithms in use (see Lipps and Vant-Hull, 1978; Mousazadeh et al., 2009; Lee et al., 2009) of which the most commonly used is the azimuth-elevation (Az-El) mount. In Az-El mount, the mirror is rotated consecutively about the azimuth and elevation angles. It was pointed out by Igel and Hughes (1979) that the astigmatic aberration of the Az-El tracking method could be reduced if the heliostats are rotated about the mirror normal in addition to the azimuth and elevation rotations thus making it a 3-DOF system. This concept later led to the development of target-aligned (T-A or spinning-elevation) heliostat where the mirror rotates about a line connecting the mirror center to the receiver (or target). The T-A method was first proposed by Ries and Schubnell (1990) and Zaibel et al. (1995) to overcome certain short comings like astigmatism, hot spots etc. of Az-El mount. Several authors (see Chen et al., 2001; Wei et al., 2011; Guo et al., 2010), independently derived the formulas for sun tracking for the T-A heliostat. Although, the T-A was developed to overcome the short comings of the Az-El method, in a comparative study of Az-El and T-A heliostats by Chen et al. (2004), it is shown that for certain times of the day and year, the Az-El performs better than T-A in terms of spillage losses and concentration.

Another exciting tracking methodology is the pitch-roll or tip-tilt using two linear actuators. Reference (Lindberg and Maki, 2010) gives a detailed account of the stress analysis in presence of gravity and wind for the pitch-roll heliostat and a complete vector-based inverse kinematic solution of the pitch-roll heliostat was provided by Freeman et al. (2017,). One of the main advantages of such a system over the Az-El is that it uses less ground space. The Stellio heliostat (Balz et al., 2016; Arbes et al., 2016) uses two linear actuators in what is called a slope-drive configuration. This type of drive eliminates the high velocity required for large change in azimuth especially when the heliostat normal reaches the vertical. Such a drive cannot be used for all heliostats in the field due to mechanical restrictions and the maximum angular distance that it can traverse is around 110°.

The two DOF parallel manipulator described in reference (Cammarata, 2015) was developed for PV systems and cannot be used for CR systems. The main reason is that for a PV system all panels in the field rotate in the same way to track the sun. However in a CR system, the heliostats are arranged around the receiver and each heliostat must rotate in a unique way to reflect the incident solar energy to the distant stationary receiver – one can intuitively see that a heliostat in the East

direction need to move differently than one in the North direction and the motion will be different depending on the distance of the heliostat from the central receiver. To the best of our knowledge there are no other parallel manipulators proposed for sun tracking in CR systems in literature.

From the literatures available, it is clear that structural weight, astigmatic aberration, spillage loss and increasing energy output by improving the pointing accuracy of the end effector are some of the major concerns among researchers across the world. This work addresses some of these issues by making use of a 3-DOF spatial parallel manipulator with three 'legs' with each 'leg' containing a passive rotary (R) joint fixed at the base, a sliding or prismatic (P) joint actuated by a linear actuator and a passive spherical (S) (ball) joint connected to the moving platform. It is shown that this 3-DOF parallel manipulator – also known as the 3-RPS manipulator – can track the apparent motion of the sun autonomously in CR systems. This parallel manipulator is chosen due to its inherent advantages such as high pointing accuracy, high stiffness, availability of parameters which can be used for optimization to reduce weight and deflection of the mirror due to wind gusts and self loading, possibility of using low cost linear actuators and avoiding large and accurate gear reduction to track the slow moving sun and ease of solving inverse kinematics for real time control. This work deals with the analysis, design, prototyping and experimental validation of a 3-RPS parallel manipulator for sun tracking in CR systems.

This paper is organized as follows: In Section 2, the geometry of the 3-RPS manipulator and the preliminaries required to understand sun tracking in CR systems are presented. It also presents the kinematic equations which form the basis of algorithm development. A detailed description of an iterative search method to obtain least structural weight and find the various design parameters which govern the actuations required and spillage loss are given in Section 3. Section 4 gives the results obtained during the simulation study conducted. Section 5 presents a detailed description of prototyping and experiments done with the 3-RPS parallel manipulator and Section 6 presents the conclusions of this work.

2. The 3-RPS parallel manipulator

Fig. 1 shows the schematic diagram of a 3-RPS heliostat reflecting the incident solar radiations to the receiver tower. The relative motion of the sun in the sky with respect to earth is known completely from the knowledge of date, time and location on the Earth's surface and hence the sun vector, $\overrightarrow{GS}$, is known. Referring to Fig. 1, let O represents the origin of a global or fixed co-ordinate system located at the base of the receiver tower and the OX, OY and OZ axes pointing towards the East, North and Zenith directions, respectively. The location of the heliostat on the surround solar field described by point O_1 is specified by the distance, R_d, from O and the angle ψ with respect to the OX axis. The base co-ordinate system at the heliostat, $\{B\}$, has its origin at O_1 and axes x_b, y_b and z_b are described with respect to the fixed coordinate system by a rotation γ about the Z axis. The platform or mirror coordinate system, $\{M\}$, is located at G with axes x_m, y_m and z_m as shown. The reference point on the platform, G, is given by the vector $\overrightarrow{O_1G}$ having co-
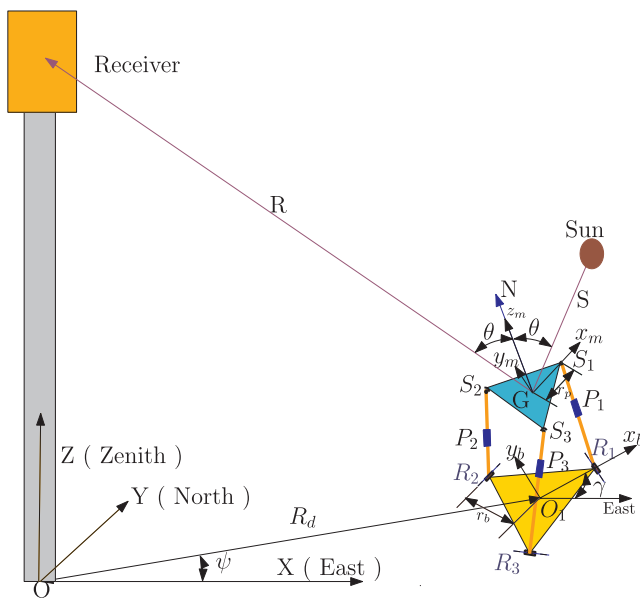
Fig. 1. Schematic of the 3-RPS parallel manipulator.

ordinates $[x_G \ y_G \ z_G]^T$ with respect to $\{B\}$. The next section describes the algorithm developed to find the actuations required for sun tracking.

2.1. Kinematics and computation of actuator motions

The kinematic equations of the 3-RPS manipulator was originally presented by Lee and Shah (1988). The modifications required to use it as a heliostat in CR systems is given in reference (Shyam and Ghosal, 2015) and is presented here in brief for completeness.

The mirror assembly in actual practice would be square or rectangular in shape but for the purpose of kinematics, only the triangles formed by R_i's and S_i's, i = 1, 2, 3, need to be considered and they are assumed to be an equilateral triangle whose circum-radii are r_b and r_p, respectively. It is known that the DOF of the 3-RPS manipulator is three and hence three actuators are required to move the top platform (Lee and Shah, 1988; Ghosal, 2006). It is also known that the three *principal motions* of the top moving platform are rotation about the X and Y axis and a linear motion along the Z axis (Srivatsan et al., 2013). As shown in Fig. 1, let $\overrightarrow{GS}$ and $\overrightarrow{GR}$ be the unit vectors representing the sun vector (representing the incident solar radiation) and the reflected ray focused onto the stationary receiver, respectively. It may be noted that the sun vector can be found out from the known azimuth and elevation angles of the sun (Reda and Andreas, 2004; Stine and Geyer, 2001). The goal in sun tracking with the 3-RPS manipulator is to move the three actuated sliding or prismatic (P) joints such that the reflected ray, $\overrightarrow{GR}$, is always focused on the receiver as the sun vector $\overrightarrow{GS}$ changes during the day and with seasons. This can be done by orienting the mirror normal, $\overrightarrow{GN}$, appropriately. From the laws of reflection, viz., a) the incident ray, reflected ray and the mirror normal should lie on the same plane and b) the angle of incidence equals the angle of reflection, the unit normal to the mirror can be found (Shyam and Ghosal, 2015) as

$$\overrightarrow{GN} = \frac{\overrightarrow{GS} + \overrightarrow{GR}}{\|\overrightarrow{GS} + \overrightarrow{GR}\|} = \begin{bmatrix} a_1 \\ a_2 \\ a_3 \end{bmatrix} \tag{1}$$

where $\|$ represents the modulus (or norm) function. For both the Az-El and T-A heliostats, the co-ordinates of the center G is fixed and known and hence the normal $\overrightarrow{GN}$ is completely known from prior knowledge of the receiver co-ordinates and the sun vector and hence the orientation of the mirror is known. For the 3-RPS, the center of the heliostat can move and is unknown and hence the normal becomes a function of

the co-ordinates of the center and the sun's azimuth and elevation angles. Secondly, for tracking the sun only two rotational degrees of freedom is enough. However, the 3-RPS has three linear actuators and hence it has a redundant degree of freedom. The redundancy and the motion of the center G makes the problem of finding the three linear actuator motion more difficult.

To obtain the desired motions of the sliding joints, we start with the transformation matrix which relate the position and orientation of the mirror with respect to the base. This can be symbolically written as

$$[T] = \begin{bmatrix} n_1 & o_1 & a_1 & x_G \\ n_2 & o_2 & a_2 & y_G \\ n_3 & o_3 & a_3 & z_G \\ 0 & 0 & 0 & 1 \end{bmatrix} \tag{2}$$

where x_G, y_G, z_G are the co-ordinates of the center point on the top platform with respect to the base, a_1, a_2, a_3 are the direction cosines of the mirror normal $\overrightarrow{GN}$ (also the local Z axis), and $n_1, n_2, n_3, o_1, o_2, o_3$ are the direction cosines of the arbitrarily chosen X and Y axis in the plane of the mirror, respectively. Since, the location of the sun in the sky is known a_1, a_2, a_3 are known and hence to solve for the 9 additional variables in $[T]$, we need to develop 9 constraint equations.

As in any 4×4 transformation matrix, we can write five constraint equations as

$$n_1^2 + n_2^2 + n_3^2 = 1$$
$$o_1^2 + o_2^2 + o_3^2 = 1$$
$$n_1 a_1 + n_2 a_2 + n_3 a_3 = 0$$
$$n_1 o_1 + n_2 o_2 + n_3 o_3 = 0$$
$$o_1 a_1 + o_2 a_2 + o_3 a_3 = 0 \tag{3}$$

To resolve the redundancy, we set

$$z_G = \text{constant} \tag{4}$$

as the orientation of the mirror is independent of its Z motion. It maybe mentioned that the Z motion can be used to pull down the mirror closer to the fixed base during high winds for safety reasons.

The normal to the mirror, $\overrightarrow{GN}$, is given by Eq. (1). From prior knowledge of the receiver co-ordinates, it can be found that the reflected ray $\overrightarrow{GR}$ is a function of x_G, y_G and the assumed value of z_G. Since $\overrightarrow{GS}$ is known completely, the normal $\overrightarrow{GN}$ is also a function x_G, y_G and the assumed value of z_G. The 3-RPS configuration introduces additional three constraints (Lee and Shah, 1988) given by

$$y_G + n_2 r_p = 0 \tag{5}$$

$$n_2 = o_1 \tag{6}$$

$$x_G = \frac{r_p}{2}(n_1 - o_2) \tag{7}$$

where r_p is the circum-radius of the top equilateral triangle. Eqs. (3), (4) and the three constraint equations given above are the 9 required equations which need to be solved to obtain all the unknown 9 quantities in the transformation matrix $[T]$.

Instead of dealing with 9 equations in 9 unknowns, we substitute Eqs. (5)–(7) in Eq. (3), to get

$$n_1^2 + \left(\frac{y_G}{r_p}\right)^2 + n_3^2 = 1 \tag{8}$$

$$\left(\frac{y_G}{r_p}\right)^2 + \left(n_1 - \frac{2x_G}{r_p}\right)^2 + o_3^2 = 1 \tag{9}$$

$$n_1 a_1 - \frac{y_G}{r_p} a_2 + n_3 a_3 = 0 \tag{10}$$

$$-2n_1 \frac{y_G}{r} + \frac{2x_G y_G}{r_p^2} + n_3 o_3 = 0 \tag{11}$$

$$\frac{-y_G}{r_p}a_1 + \left(n_1 - \frac{2x_G}{r_p}\right)a_2 + o_3a_3 = 0 \tag{12}$$

Thus we arrive at 5 equations in 5 unknowns, viz., n_1, n_3, o_3, x_G and y_G which can be numerically solved using MATLAB® (MATLAB, 2012) provided function *fsolve*. Once these 5 unknowns are solved for, the remaining three can be obtained from the earlier step and with the chosen z_G, the complete $[T]$ matrix is known for a given sun vector $\overrightarrow{GS}$.

From the geometry of the 3-RPS manipulator, the co-ordinates of the rotary joints with respect to $\{B\}$ are given by $\overrightarrow{O_1R_1} = [r_b, 0, 0]^T$, $\overrightarrow{O_1R_2} = \left[-\frac{1}{2}r_b, \frac{\sqrt{3}}{2}r_b, 0\right]^T$ and $\overrightarrow{O_1R_3} = \left[-\frac{1}{2}r_b, -\frac{\sqrt{3}}{2}r_b, 0\right]^T$ and the co-ordinates of the spherical joints with respect to $\{M\}$ are given by $\overrightarrow{GS_1} = [r_p, 0, 0]^T$, $\overrightarrow{GS_2} = \left[-\frac{1}{2}r_p, \frac{\sqrt{3}}{2}r_p, 0\right]^T$ and $\overrightarrow{GS_3} = \left[-\frac{1}{2}r_p, -\frac{\sqrt{3}}{2}r_p, 0\right]^T$. The position vector of the spherical joints S_i ($i = 1, 2, 3$) with respect to the co-ordinate system $\{B\}$ is given as

$$\begin{bmatrix} \overrightarrow{O_1S_i} \\ 1 \end{bmatrix} = [T]\begin{bmatrix} \overrightarrow{GS_i} \\ 1 \end{bmatrix}$$

where $[T]$ is now known.

The actuations l_i, $i = 1,2,3$ needed to achieve the desired transformation matrix $[T]$ can be found out as (Ghosal, 2006)

$$l_i = ||\overrightarrow{O_1R_i} - \overrightarrow{O_1S_i}|| \tag{13}$$

This completes the solution of the inverse kinematics problem of the 3-RPS parallel manipulator used to track the sun in CR systems.

It has also been found that the orientation of the $\{B\}$ with respect to the fixed co-ordinate system has a major effect on the spillage loss (see also simulation results in Section 4). The one extra DOF in the 3-RPS heliostat enables it to attain orientations which are equivalent to rotating the Az-El heliostats about the mirror normal. In other words, it can be seen that

$$[R_{Az-El}]^T[R]_{3-RPS} = \begin{bmatrix} \cos(\kappa) & -\sin(\kappa) & 0 \\ \sin(\kappa) & \cos(\kappa) & 0 \\ 0 & 0 & 1 \end{bmatrix}$$

where $[R]$ denotes the rotation matrix of Az-El and 3-RPS heliostats and ^{T} denotes the transpose of the matrix. Thus the astigmatic aberration which is the spread of solar image on the receiver aperture will be reduced in the 3-RPS heliostat.

3. Design of the 3-RPS heliostat

The mirror has to be attached to a support frame to prevent it from excessive deformation during wind gusts and loading due to gravity. Various frame topologies have been considered for 3-RPS and are shown in Fig. 2. The aim is to obtain the lightest possible support structure which satisfies the beam error criterion of 2–3 mrad during the acceptable operational wind speed. It is to be noted that the value of wind speed used depends upon the geographic location. The wind load, P, can be calculated using the equation

$$P = \frac{1}{2}C_d\rho v^2 FoS \tag{14}$$

where $C_d = 1.18$ is the aero-dynamic drag coefficient, ρ is the density of air, v is the wind speed and FoS is a factor of safety used to take into account uncertainties. It may be mentioned that the reduction in weight of the support structure helps in reducing the overall cost of the heliostat. The details regarding parametric CAD modeling and finite element analysis to obtain the lightest possible structure is reported in (Shyam and Ghosal, 2015). The percentage reduction in structural weight varies from 15–60% for small (2 m × 2 m) to large mirrors (5 m × 5 m) respectively.

The 3-RPS heliostat has several design parameters. The main ones are r_b and r_p denoting the base and top circum-radii respectively. Additionally we have the angle γ which denotes the orientation of the x_b axis with respect to the local East direction. The availability of these parameters allows us to search for an optimum design of the 3-RPS heliostat and this is presented in the rest of the section. It maybe noted that no such design parameters and hence the possibility of optimization exists in the traditional Az-El and T-A configurations.

3.1. Iterative search for design parameters

We begin by searching for the optimum value of γ which decides the orientation of the base platform with respect to the global axis.

3.1.1. Optimum γ

It is found from simulations that varying the parameter γ, the spillage loss can be minimized. To study the effect of γ, extensive numerical simulation by varying γ in steps has been carried out (refer Section 4 for details) and it was found that $\gamma = \psi$ or $\gamma = \psi + 180°$ not only minimizes the spillage loss but also reduces the actuations required for the 3-RPS heliostat to track the sun.

3.1.2. Search for r_p

The connection points at the top platform defined by the length r_p from the center, G, has two significant effects. As r_p increases, the stroke required to get the same orientation of the mirror increases. The other effect is that a large value for r_p tends to increase the deformation of the mirror at the center due to wind and gravity loading whereas a small value corresponds to large deformation at the edges. Of the above two, the most critical criteria is on the deformation which needs to be within a beam error limit of 2–3 mrad. Hence a finite element analysis is carried out to find out the deflections by varying r_p iteratively. For 2 m × 2 m, 3 m × 3 m and 5 m × 5 m mirror, the value of r_p thus obtained are 500, 900 and 1800 mm, respectively. Similar analysis and optimized r_p can be found for mirrors of other sizes.

3.1.3. Search for r_b

The optimum r_b depends on the height of the tower, distances and angles between the heliostat and the receiver. We have developed a general program to obtain optimum r_b where these quantities can be
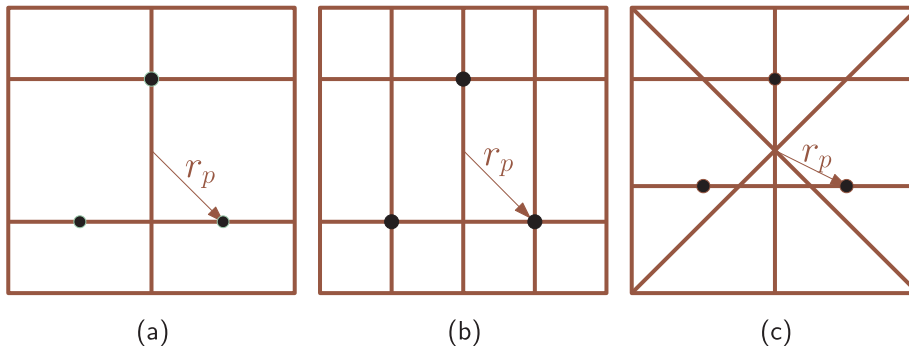

Fig. 2. Various types of frame topologies considered for 3RPS heliostat.

(a) (b) (c)

given as input. In this simulation, we have assumed that the heliostats are placed in a circular field with the nearest being 50 m away and the farthest 300 m in steps of 5 m. The angle ψ is varied from 0 to 350° in steps of 10°. To find the optimum r_b, we simulate the motion of the heliostat for three days, viz. the two solstices and any one of the equinoxes, as they give the extreme values. Depending upon the direction of incoming sun rays, the actuation required are extreme for the heliostats which are nearest and farthest from the receiver tower compared to the heliostats in between. Hence the analysis is done only for an array of heliostats at radii of 50 m and 300 m. Initially, the heliostat is parallel with the ground plane and is considered to be the zero actuation or in the stow position. Actuations above and below zero are considered positive and negative, respectively. For any other orientation, the point on the ground where the perpendicular dropped from the connection point meets, gives the position of r_b for least actuation required. Since the heliostat is required to have several orientations to track the sun, r_b changes with time. It is also found that for each ψ, the value of r_b which minimizes the stroke is not a constant value. Since it is practically impossible to make different types of heliostats at different locations, the mean value of r_b is chosen as the optimal value. With the above considerations, the optimal value of r_b is found to be 487 mm, 877 mm and 1755 mm for a 2 m × 2 m, 3 m × 3 m and 5 m × 5 m mirror size, respectively. The r_p and r_b thus obtained ensures that the stroke of the linear actuator is less than 700 mm.[1]

4. Simulation results

We have performed extensive simulations to obtain the various parameters in the design of the heliostat. In this section we present the simulations done for Bangalore (12°58′13″N, 77°33′37″E), India for four different days, viz., the March equinox, summer solstice, September equinox and winter solstice (The equinoxes would give the same simulation result). For the simulations, the commercial software MATLAB® is used. The inputs required for the simulation are chosen as follows.

The center co-ordinates of the receiver tower with respect to the global coordinate system is $[0\ 0\ 65\ \text{m}]^T$. The heliostat is placed at a radial location of 100 m from the receiver tower and at 30° from the nominal East direction. The value assumed for z_G is 2 m from the center of the bottom platform. Initially, both the top and bottom platforms of the 3-RPS heliostat are assumed to be parallel. The size of mirror or receiver is not a restriction to the program that we have developed. However, the simulations carried out in this section are for a mirror dimension of 2 m × 2 m and a receiver dimension of 2.5 m × 2.5 m. Fig. 3 shows the simulations done for March equinox at Bangalore. It can be seen from these figures that the 3-RPS manipulator do not attain any singular configurations. Extensive simulations have been done for different latitudes and locations to verify this fact and found that this holds true. Fig. 4 gives the actuation required for the three legs of the 3-RPS manipulator, at the chosen location (radial distance of 100 m from the receiver tower and at 30° from the nominal East direction) in the field to track the sun for equinoxes and solstices in Bangalore. Fig. 5 gives the variation of the center of the moving platform for equinoxes and solstices in Bangalore. It is clear from the plots that the x_G and y_G motion of the center is very small and is in the range of ± 0.1 m (z_G is assumed constant and is equal to 2 m), i.e., the footprint of the mirror remains essentially over the base.

For obtaining an estimate of the spillage losses, it is assumed that

the sun rays hitting the center of the mirror are reflected to centre of the receiver aperture at every instant of time. Additionally, the mirror is assumed to be flat and the sun is considered as a point source. Hence, the parallel sun rays hitting the four corners of the mirror will be reflected to the receiver aperture parallel to the central ray. The points where the reflected rays from the mirror corner hit the receiver aperture are joined together to form the image polygon. As the sun moves across the sky and the mirror rotates, the image polygon rotates and at some instants of time, a portion of the image polygon is outside the assumed receiver area and this area is used as an estimate of the spillage loss.[2] This area is calculated for every one minute interval from 7 a.m. to 6 p.m. and is shown in Fig. 6 for the Az-El, T-A and 3-RPS heliostat at different time of the day. Fig. 7 shows the spillage loss for all the three different types of heliostat when kept at various angles in a 360° surround solar field in Bangalore. It can be seen from the figures that there are occasions when one type of heliostat performs better compared to the others from the point of view of spillage loss. It is also clear from Fig. 7 that the spillage loss for the 3-RPS heliostat is large for locations other than $\psi = 0$ and 180° when compared to the Az-El and T-A heliostats. The above analysis assumes that the base and the global co-ordinate system are parallel to each other or the rotation matrix associated with it is identity. For 3-RPS, by changing the orientation of base with respect to global co-ordinate system (a rotation about Z axis by an angle γ as in Fig. 1), it is found that there is considerable amount of reduction in spillage loss as shown in Fig. 8. To reduce the spillage loss, the area under the curve, with units m²-hr, in Fig. 8 needs to be minimized. This area under the curve, for various values of γ's, is shown in Fig. 9 and it can be clearly seen from Fig. 9 that the minimum occurs at four values of γ which are 90° apart. Simulations have also been carried out for various locations in the field and it has been found that the minimum spillage loss occurs at places corresponding to $\gamma = \psi, \psi + 90, \psi + 180, \psi + 270$. Fig. 10 shows the spillage loss when $\gamma = \psi$ for the 3-RPS heliostat.

Fig. 11 shows in blue color the actuations required in the upward direction from the home position where the plane of the mirror is parallel to the ground. This is indicated as a positive value. The red color indicates the actuations in the downward direction from the home position which is given as a negative value. The sum of the absolute values of the blue and red gives the total actuation required. It is clear from Fig. 11 that for this particular location (100 m and 30⁰) with $\gamma = \psi + 180$ gives the least actuation. It can be verified from other simulations that $\gamma = \psi$ or $\gamma = \psi + 180$ always minimize the stroke.

5. Experimental validation of the 3-RPS heliostat

To validate the theory developed in the previous section, we fabricated a 3-RPS heliostat and to compare the sun tracking ability of the 3-RPS heliostat, we also fabricated an Az-El heliostat. Details of the prototype are presented in this section. In the next section, we present the experimental results and a comparison.

5.1. Prototype design

A prototype of the 3-RPS parallel manipulator with a mirror dimension of 1 m × 1 m has been made and is shown in Fig. 12. The mirror is enclosed in an aluminum frame at its edges having rubber beadings separating the frame and the mirror. This will ensure a tight fit between the two and also avoids any scratches on the mirror. The aluminum frame is rigidly attached to the support structure using L angles. The bottom platform is made of mild steel having a dimension of 1 m × 1 m × 5 mm. This is made heavy to prevent the heliostat from toppling over in presence of gusty winds but in a real power plant, it is

---

[1] As the stroke length increases, the chances of buckling and other modes of failure increases. Additionally, it is easier to obtain linear actuator with smaller strokes. The stroke of 700 mm mentioned here was chosen since we could easily obtain such a linear actuator. This stroke is for the particular heliostat dimension considered for the study, viz., up to 5 m × 5 m and for the other chosen field parameters. The search method that we have developed can be easily used to find out the stroke for any other heliostat dimension.

[2] A more accurate measure of spillage loss need to include the spot shape, size and aberrations due to astigmatism as mentioned in reference (Chen et al., 2004).
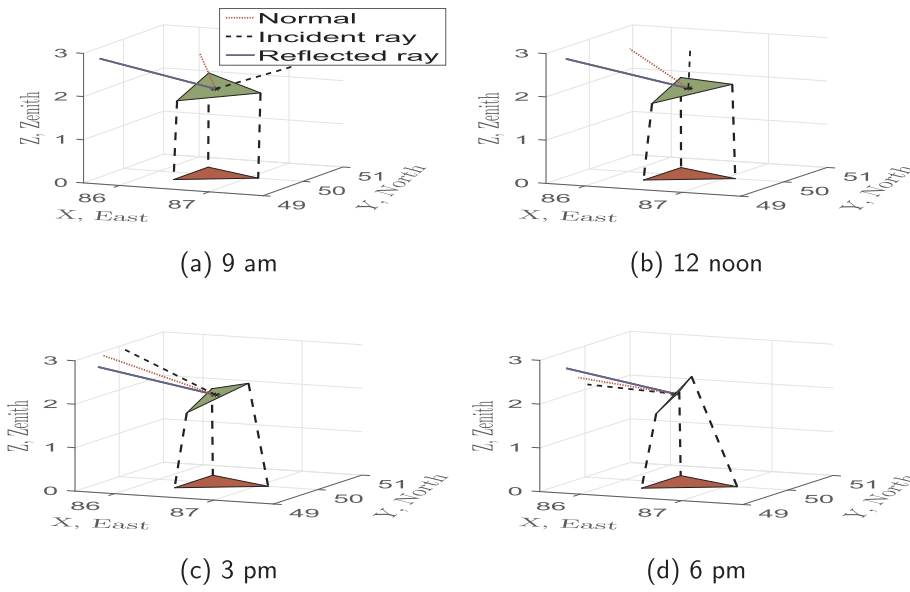
(a) 9 am

(b) 12 noon

(c) 3 pm

(d) 6 pm

Fig. 3. Simulation of 3-RPS heliostat for March equinox for Bangalore.

(a) March equinox

(b) Summer solstice

(c) September equinox

(d) Winter solstice
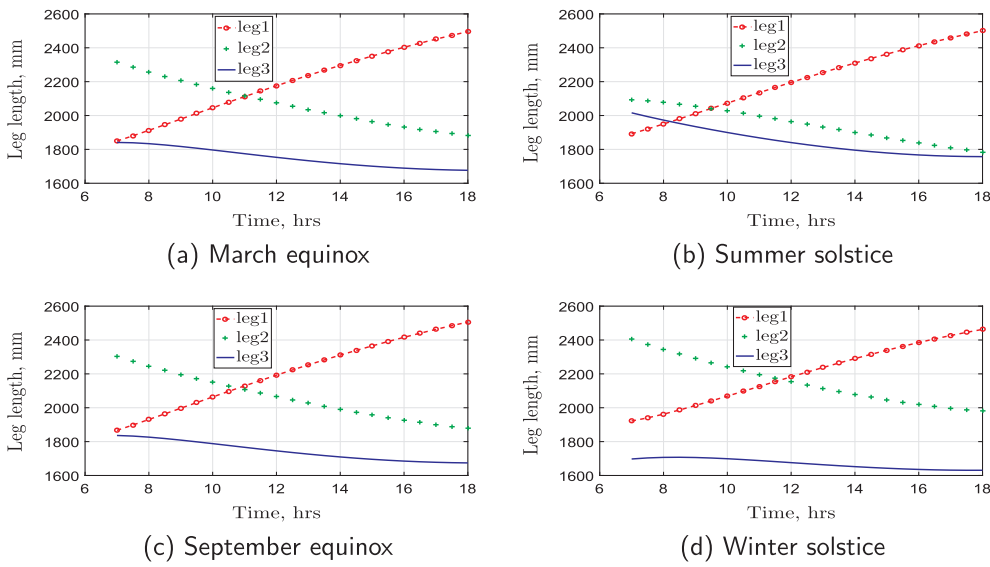
Fig. 4. Actuations required for the 2 m × 2 m 3-RPS heliostat in Bangalore.

(a) March equinox

(b) Summer solstice

(c) September equinox

(d) Winter solstice
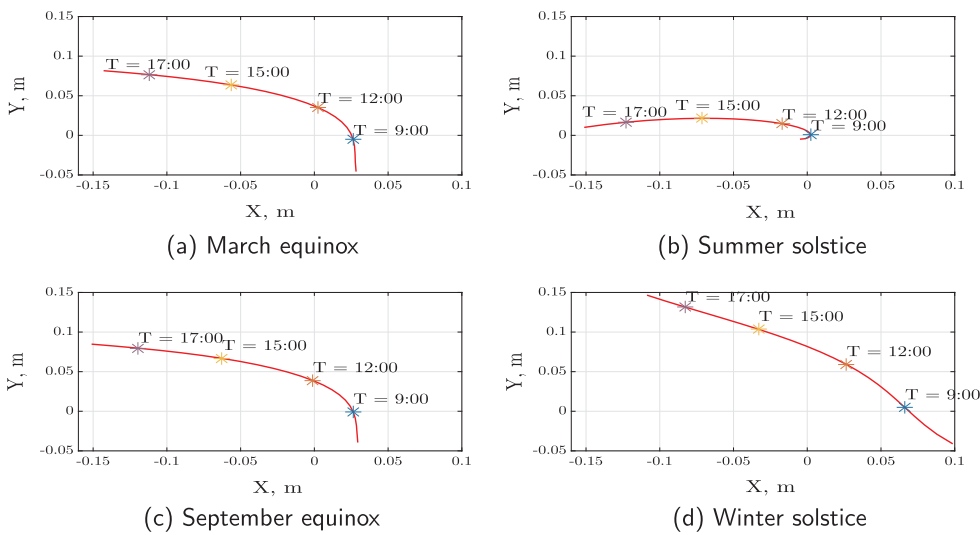
Fig. 5. Variation of the center of 2 m × 2 m 3-RPS heliostat in Bangalore.
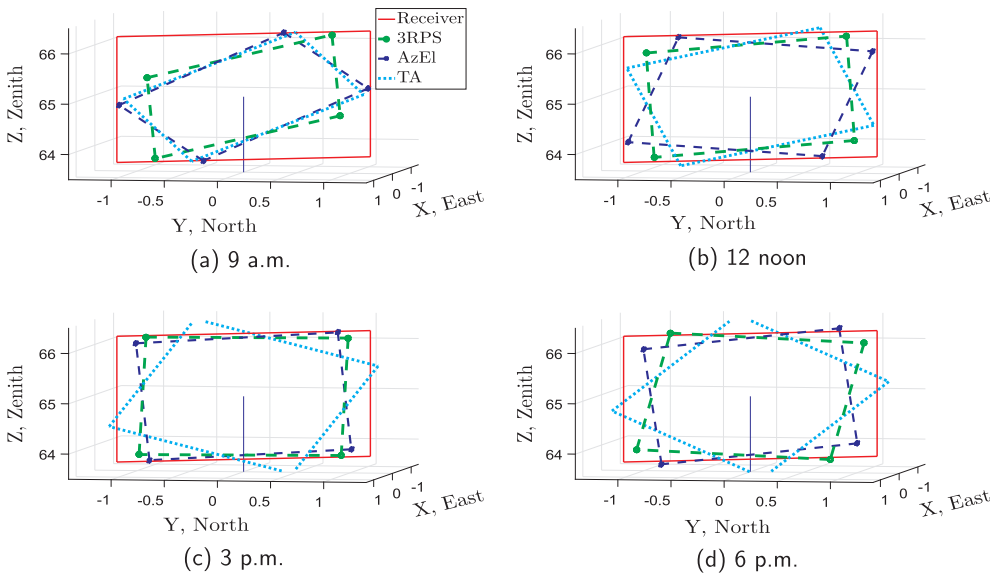
Fig. 6. The image on the receiver aperture for a 2 m × 2 m mirror on a 2.5 m × 2.5 m receiver at various time instants for March equinox at Bangalore.

recommended that the rotary joints of the actuators to be fixed to the ground with concrete. Supports are also provided at the edges for ease of handling. The support frame is made of mild steel. The cross section of the support frame has a dimension of 20 mm × 20 mm × 2 mm which is obtained from the finite element analysis as given in reference (Shyam and Ghosal, 2015). It is made such that the deflection should not exceed 2 mrad at the edges. Each of the linear actuators are capable of carrying a load of 1500 N with a stroke of 1000 mm. This has been designed in this way to ensure that any future modifications to the heliostat, such as using a bigger mirror, can be accomplished with the same sliding joints. Two separate attachments are also made to attach the spherical joints between the support frame and the sliding joint. These attachments are connected sufficiently rigid so that no motion except the rotation of the spherical joints happen.

5.2. Control strategy

Literature gives both open-loop (Baheti and Scott, 1980; Jones and Stone, 1999) and closed-loop control of heliostats (see, for example, (Kribus et al., 2004; Quero et al., 2007; Delgado et al., 2012; Berenguel et al., 2004)). The open-loop control relies mainly on the prior knowledge of the sun vector and receiver co-ordinates and positioning the mirror normal as the angle bisector between the two using feedback from the encoders of the motor. The closed loop-control is mainly based on feedback from some kind of sun sensor (using photo-diodes as in (Quero et al., 2007; Delgado et al., 2012)) or from cameras. In this work open-loop control strategy is implemented.

Intermittent tracking, which refers to the tracking of sun in discrete time steps is employed in this work. The time where the heliostats are kept idle is a function of the distance of the heliostat from the receiver tower, the size of the mirror and the receiver aperture. More the distance, less the idling time since as the sun moves across the sky, the reflected beam from the farthest heliostat will move the most and go outside the receiver area. From extensive simulation, it was found that for a 2 m × 2 m heliostat at a distance of 100 m from the receiver of size 2.5 m × 2.5 m, the idle time would be about 30 s. In our experiments, since the distance is small we could keep the idle time much larger.

Each of the three linear actuators in the 3-RPS parallel manipulator consist of a DC motor, a gearbox and a lead screw. The pitch of the lead screw was 1 mm. For sun tracking, the actuators need to be moved either forward or backward to get the desired orientation of the mirror. In order to facilitate the forward and backward motion of the actuators, an H-bridge circuit was used. The supply voltage for the actuators is

24 V and the maximum rated current is 3.5 A.

We used a commonly used proportional, integral plus derivative (PID) control to move the actuator. The PID control scheme was implemented on a ATMEGA2560 micro-controller. A quadrature type optical encoder is used for feedback. The encoder pulses can be read and converted to linear motion of the actuator by multiplying it with an appropriate gain constant having units of distance moved per count.

To obtain the controller gains, a MATLAB-Simulink model, shown in Fig. 13, was created. A built in PID controller block is used and the transfer function of the PID block is given by Eq. (15)

$$V(s) = K_p + \frac{K_i}{s} + K_d \frac{N}{1 + N\frac{1}{s}} \tag{15}$$

where N is a filter co-efficient and the proportional gain (K_p), the integral gain (K_i) and the derivative gain (K_d) were adjusted to get the best result. The input to the PID block is the error or the difference between the desired and actual trajectory followed. The output of the PID block is a voltage, obtained using Eq. (15), and is fed to the actuator subsystem. The actuator subsystem consists of two parts – the actuator part and the feedback/encoder part. A MATLAB function block is used to route voltage thus giving directions to the actuator for its travel depending on whether the input is positive or negative. In the actual implementation, the safety of ATMEGA2560 micro-controller is ensured from the high voltage motor side by using an opto-isolator which is not modeled in the MATLAB-Simulink model. From extensive simulations, the value of N was chosen as 100 and for K_p, K_d, K_i, the values chosen were 8, 0.7 and 0.09, respectively.

Before proceeding with actual sun-tracking, the verification of algorithm was carried out in the lab. A He-Ne laser served as light source and various predefined points marked on the wall served as targets. The legs are actuated according to the inverse kinematics equations derived in Section 2.1, and it was found that the maximum error in the reflected beam was 7.1 mrad. This also validated the choice of the controller gains obtained from simulations.

5.3. Actual sun tracking

The actual sun tracking experiment was carried out on the roof of the Interdisciplinary Center for Energy Research (ICER) at IISc Bangalore for two days, viz., October 15 and November 10, 2016. The main aim of the experiments were to test if the algorithm developed was able to reflect the incident solar radiations to the receiver screen at every tracking instant. A prototype of the Az-El heliostat having the
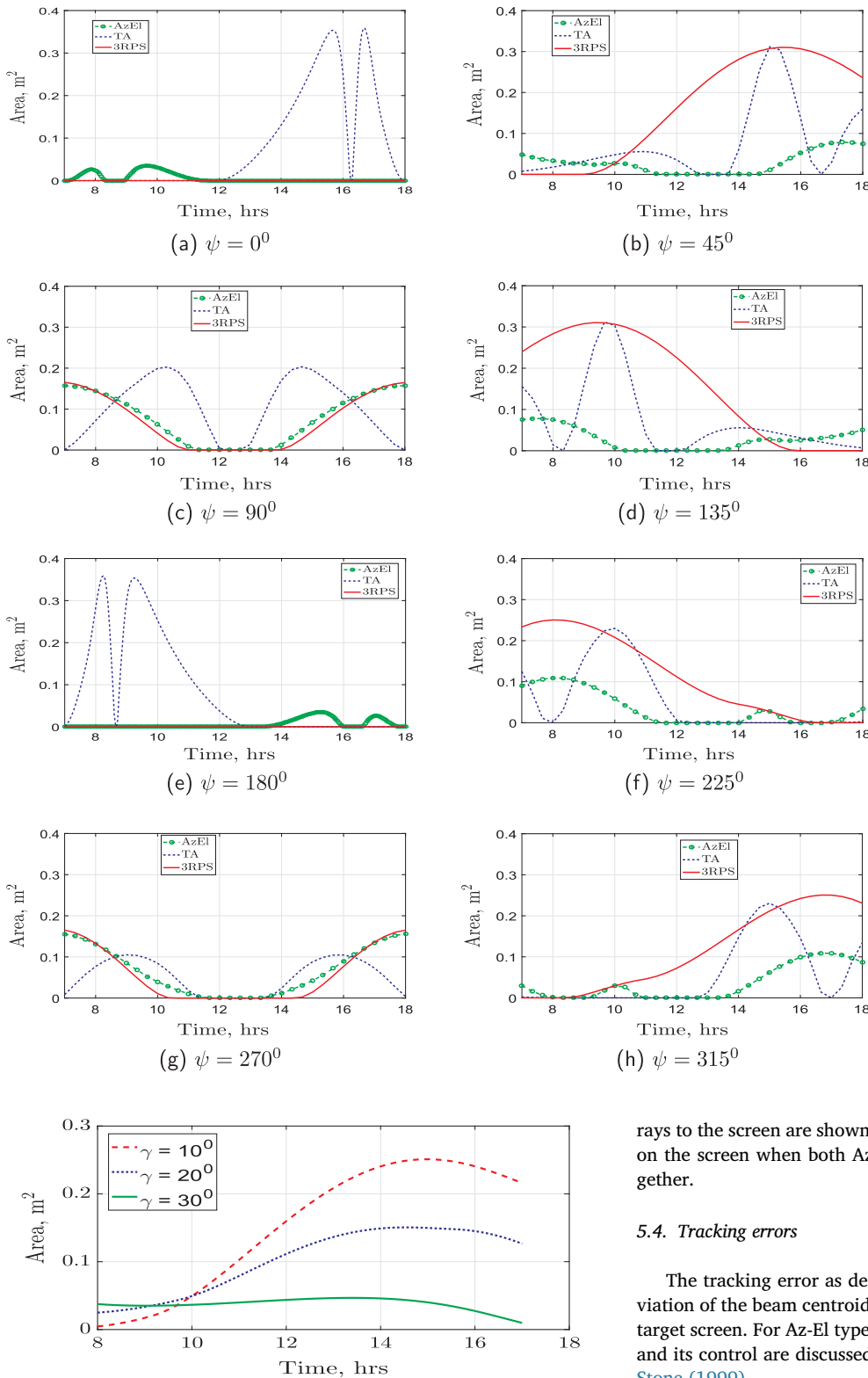
(a) $\psi = 0^0$

(b) $\psi = 45^0$

(c) $\psi = 90^0$

(d) $\psi = 135^0$

(e) $\psi = 180^0$

(f) $\psi = 225^0$

(g) $\psi = 270^0$

(h) $\psi = 315^0$

Fig. 7. Comparison of Az-El, T-A and 3-RPS with respect to spillage loss (March equinox, Bangalore for a point sun with no heliostat errors).

Fig. 8. Variation of spillage loss with γ for $2\,\text{m} \times 2\,\text{m}$ 3-RPS for March equinox, Bangalore.

same mirror dimension of 1 m × 1 m was also made for the purpose of comparison. Table 1 gives the co-ordinates of the Az-El and 3-RPS heliostats with respect to global co-ordinate system (gcs). In the table, O_1, R and z_G refers to the origin of the base coordinate system, center of the receiver and the vertical distance from O_1 to the center of the mirror co-ordinate system. The images of the 3-RPS heliostat reflecting the sun

rays to the screen are shown in Fig. 14. Fig. 15 shows the image formed on the screen when both Az-El and 3-RPS heliostats were working together.

5.4. Tracking errors

The tracking error as defined by King and Arvizu (1981) is the deviation of the beam centroid location from the desired aim-point on the target screen. For Az-El type of heliostats, the sources of tracking errors and its control are discussed in Baheti and Scott (1980) and Jones and Stone (1999).

5.4.1. Analytical expression for error

Denoting the incident, reflected and mirror normal by $\hat{i}, \hat{r}$ and $\hat{n}$, it is straight forward from the laws of optics, that

$$\hat{r} = (\hat{i} \cdot \hat{n})\hat{n} - (\hat{i} - (\hat{i} \cdot \hat{n})\hat{n})$$
$$= 2(\hat{i} \cdot \hat{n})\hat{n} - \hat{i}$$

if $\hat{n}$ changes to $\hat{n_1}$ where $\hat{n_1} = \hat{n} + \delta\hat{n}$, then the change in $\hat{r}$ can be written as
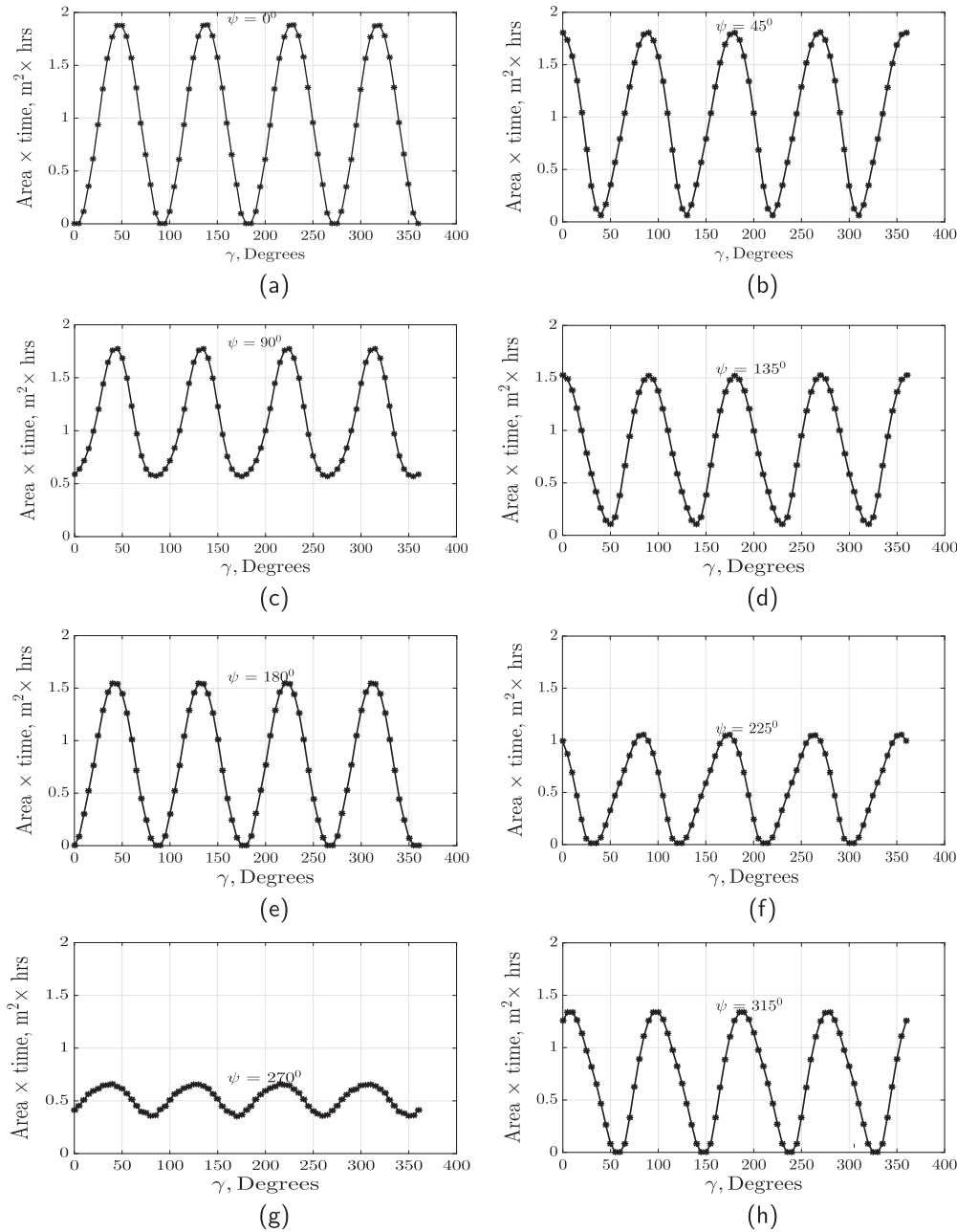
$$\Delta r = 2((\hat{i} \cdot \hat{n}_1)\hat{n}_1 - (\hat{i} \cdot \hat{n})\hat{n})$$

In Fig. 16, P is the centre of the receiver (the ideal aim-point), P_1 is the point where the reflected ray hits the receiver when errors are present, G is the centre of the reflector. We can write

$$\overrightarrow{OG} + C_1\hat{r} = \overrightarrow{OP}$$

$$\overrightarrow{OG} + C_1\hat{n}_1 = \overrightarrow{OP_1}$$

$$C_1\Delta r = \overrightarrow{OP_1} - \overrightarrow{OP}$$

$$2C_1((\hat{i} \cdot \hat{n}_1)\hat{n}_1 - (\hat{i} \cdot \hat{n})\hat{n}) = \overrightarrow{OP_1} - \overrightarrow{OP} = \begin{bmatrix} \Delta x \\ \Delta y \\ \Delta z \end{bmatrix} \tag{16}$$

where C_1 is a constant.

For Az-El method, the incident ray and normals would be

$$\hat{i} = \begin{bmatrix} \cos\alpha_s\cos\phi_s \\ \cos\alpha_s\sin\phi_s \\ \sin\alpha_s \end{bmatrix}; \hat{n} = \begin{bmatrix} \cos\alpha_n\cos\phi_n \\ \cos\alpha_n\sin\phi_n \\ \sin\alpha_n \end{bmatrix};$$

$$\hat{n}_1 = \begin{bmatrix} \cos(\alpha_n + \Delta\alpha_n)\cos(\phi_n + \Delta\phi_n) \\ \cos(\alpha_n + \Delta\alpha_n)\sin(\phi_n + \Delta\phi_n) \\ \sin(\alpha_n + \Delta\alpha_n) \end{bmatrix}$$

where α and ϕ are the elevation (measured from ground plane) and azimuth (measured from X axis) angles of the sun vector and normal indicated by the suffixes s and n, respectively.

For the 3-RPS, in terms of the joint space variables, the coordinates of the spherical joints with respect to the base co-ordinate system, {B}, can be written as (see Fig. 1) as

$$O_1S_1 = \begin{bmatrix} r_b - l_1\cos\theta_1 \\ 0 \\ l_1\sin\theta_1 \end{bmatrix}; O_1S_2 = \begin{bmatrix} -0.5(r_b - l_2\cos\theta_2) \\ \frac{\sqrt{3}}{2}(r_b - l_2\cos\theta_2) \\ l_2\sin\theta_2 \end{bmatrix}; \tag{17}$$

(a) $\psi = 0^0$

(b) $\psi = 45^0$

(c) $\psi = 90^0$

(d) $\psi = 135^0$

(e) $\psi = 180^0$

(f) $\psi = 225^0$

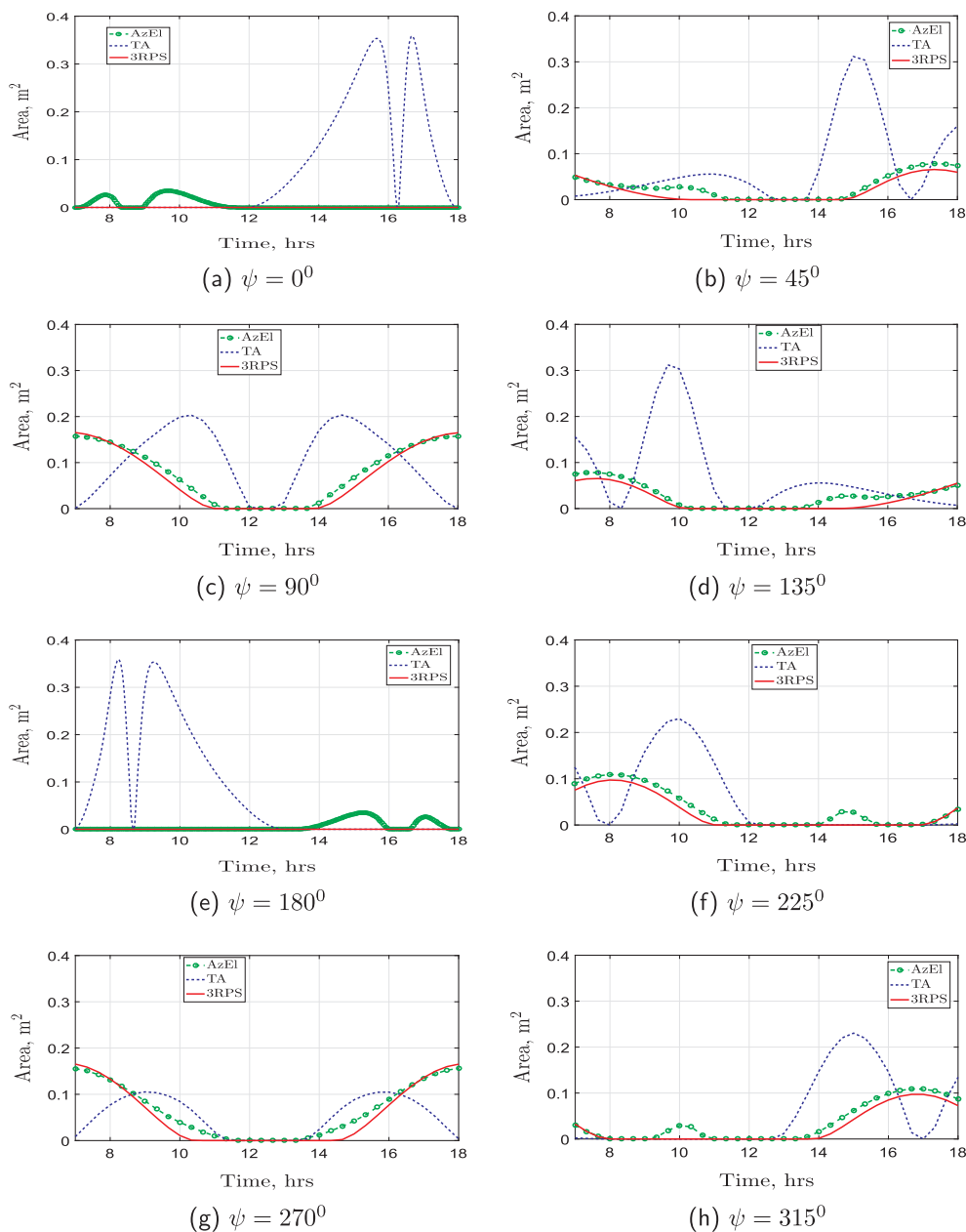(g) $\psi = 270^0$

(h) $\psi = 315^0$

Fig. 10. Comparison of Az-El, T-A and 3-RPS with respect to spillage loss, $\gamma = \psi$ March equinox, Bangalore.

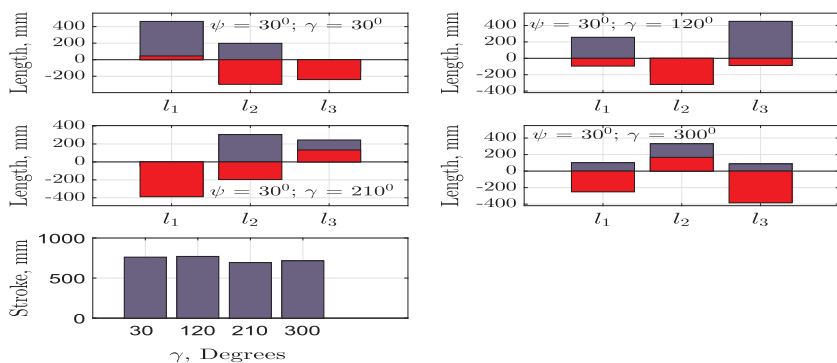**Fig. 11.** Variation of leg lengths l_1, l_2 and l_3 with γ for March equinox, Bangalore.
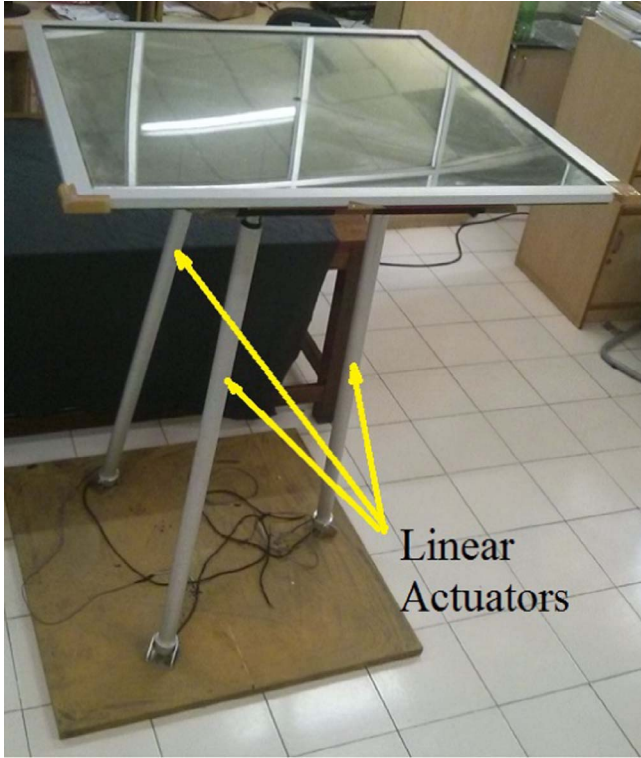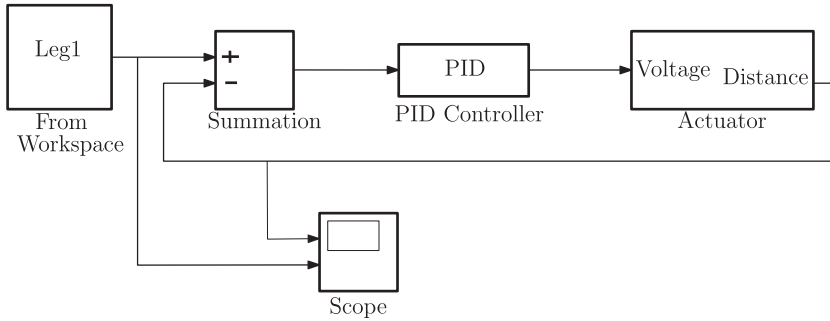
Fig. 12. Prototype of 3-RPS heliostat.

$$O_1 S_2' = \begin{bmatrix} -0.5(r_b - (l_2 + \Delta l_2)\cos\theta_2) \\ \frac{\sqrt{3}}{2}(r_b - (l_2 + \Delta l_2)\cos\theta_2) \\ (l_2 + \Delta l_2)\sin\theta_2 \end{bmatrix};$$

$$O_1 S_3' = \begin{bmatrix} -0.5(r_b - (l_3 + \Delta l_3)\cos\theta_3) \\ -\frac{\sqrt{3}}{2}(r_b - (l_3 + \Delta l_3)\cos\theta_3) \\ (l_3 + \Delta l_3)\sin\theta_3 \end{bmatrix}$$

where the θ_i (i = 1, 2, 3) are the angles that the legs make with the base platform. Here, the incident ray would remain same as in Eq. (16) but the normals would be different and could be found out as

$$\hat{n} = [R]\frac{(O_1 S_2 - O_1 S_1) \times (O_1 S_3 - O_1 S_1)}{\| (O_1 S_2 - O_1 S_1) \times (O_1 S_3 - O_1 S_1) \|}$$

$$\hat{n}_1 = [R]\frac{(O_1 S_2' - O_1 S_1') \times (O_1 S_3' - O_1 S_1')}{\| (O_1 S_2' - O_1 S_1') \times (O_1 S_3' - O_1 S_1') \|}$$

where $[R]$ is the rotation matrix which takes the base co-ordinate system to the global co-ordinate system and Eq. (16) could be used to find out the error. In the expressions above, Δ indicates a small change in the respective quantity. It is also assumed the motion of the centre of the 3-RPS heliostat is negligible. Fig. 17 shows the error vector, ϵ, from the actual image where R is the centre of the receiver and C_i is the centroid of the reflected image. The point C_i is found by image processing. The error vector, ϵ is resolved into its components along north and zenith axes. The component along North axis divided by the slant height gives the horizontal error in radian. Similarly, the component along zenith divided by slant height gives the vertical error. Figs. 18 and 19 respectively give the error bar plots of 3-RPS and Az-El heliostats.

Fig. 13. Schematic of the control strategy used.

Table 1
Location parameters of Az-El and 3-RPS heliostats wrt gcs.

	$\mathscr{O}_1[\mathbf{x\ y\ z}]^T\ \mathbf{m}$	$\mathbf{R}\ [\mathbf{x\ y\ z}]^T\mathbf{m}$	z_G
Az-El	[−14 5.45 0]	[0 0 6.72]	1.58
3-RPS	[−14 3.45 0]	[0 0 6.72]	1.64

$$O_1 S_3 = \begin{bmatrix} -0.5(r_b - l_3\cos\theta_3) \\ -\frac{\sqrt{3}}{2}(r_b - l_3\cos\theta_3) \\ l_3\sin\theta_3 \end{bmatrix}$$

$$O_1 S_1' = \begin{bmatrix} r_b - (l_1 + \Delta l_1)\cos\theta_1 \\ 0 \\ (l_1 + \Delta l_1)\sin\theta_1 \end{bmatrix};$$

(18)

From the error plots, we can see that the average error in horizontal and vertical directions for the 3-RPS configuration is 30.7 mrad and 34.3 mrad respectively where as the same for Az-EL configuration is 21.3 mrad and 19.0 mrad.

5.5. Comparison of spillage loss

For November 10, the spillage loss obtained from simulations is shown in Fig. 20. Fig. 21 shows the photographs taken on the same day when both Az-El heliostats were working together. It is clear from the Fig. 21 that the deviation of the image from the aim-point on the screen is more for the Az-El heliostat compared to the 3-RPS heliostat. To showcase the images on the receiver more clearly background is darkened intentionally.

5.6. Key observations made during the prototype validation

We present some of the other observations made during experimentation.

- It was observed that for the prototype Az-El heliostat with two motors, a torque has to be always applied to hold the mirror at a particular orientation. Hence some energy is spent even while the

(a) 11 a.m.

(b) 12 noon

(c) Cloudy

(d) 03:30 p.m.

Fig. 14. The image formed on the screen using 3-RPS heliostat on October 15, 2016.

(a) 11:15 a.m.

(b) 12 noon

(c) Almost cloudy

(d) 03:30 p.m.

Fig. 15. The image formed on the screen when Az-El and 3-RPS were working together on October 15, 2016.

heliostat is held stationary at one particular orientation.[3] In the 3-RPS, the weight of the mirror is supported by actuators which are not back drivable and hence no energy is spent when the heliostat is stationary.

- The cone angle of the spherical joints used in the prototype is found to be ± 32°. This makes it impossible for the 3-RPS heliostat to track the sun when it is kept very close to the receiver. A spherical joint with larger cone angle is required in such situations.
- There was some play in the rotary joints in the 3-RPS heliostat and as a result the pointing error is more than the Az-El heliostat. This

can be overcome by better manufacturing and choice of the rotary joints. The accuracy of tracking is also dependent on how precisely the coordinates of the heliostat in the field and the receiver tower are found out with respect to the global coordinate system. In the lab such determination was very accurately done and hence the error in the lab experiments were smaller – 7.1 mrad. A precise notion of the direction of East and Zenith and the sun's path calculated using the station coordinates, day of the year and time are also required for improving the tracking accuracy. These are the other possible reasons why the errors in tracking are more in the experiments done on the roof of the building.

Nevertheless, the experimental results presented in this section

---

[3] If a linear actuator which is not back drivable is used (as in the Stellio heliostat), then no energy will be spent for maintaining the orientation.
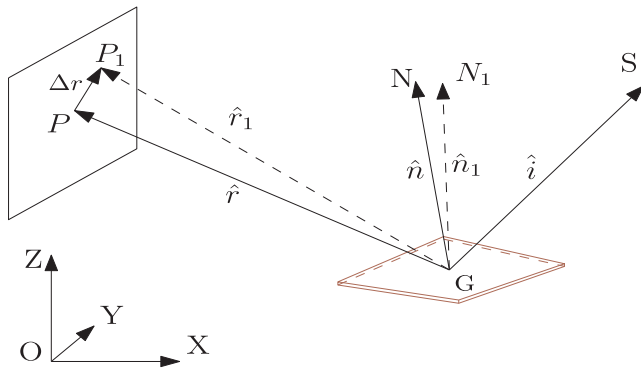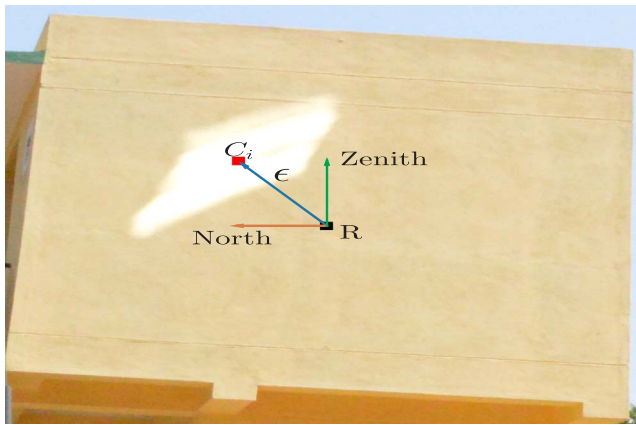
Fig. 16. Tracking error.

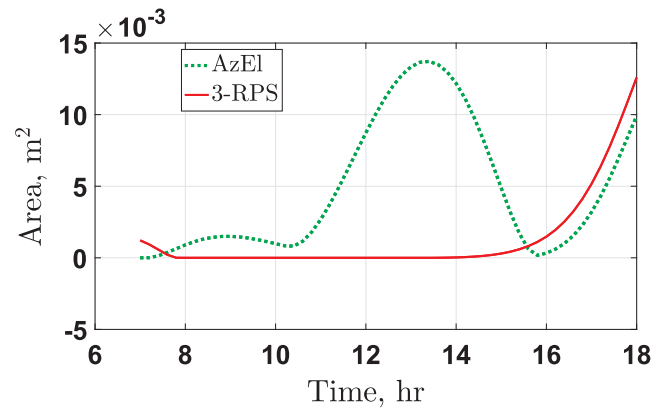**Fig. 17.** Actual photograph showing the tracking error.

Fig. 20. Spillage loss comparison for Az-El and 3-RPS heliostat on November 10th.

clearly demonstrate that the 3-RPS heliostat can track the sun with an accuracy similar to the Az-El heliostat.

6. Conclusion

This paper presents in detail the kinematic modeling, simulation, design and experimental investigation on a novel 3-RPS parallel manipulator based heliostat to track the sun for a central receiver tower based concentrated solar power station. The 3-RPS parallel manipulator supports the end-effector (mirror) at three points and hence can support larger mirrors with less deflection in presence of wind and gravity loading. From the analysis it has been shown that for a given mirror size and a desired deflection at the edge, the supporting structure weight can be as much 60% less when compared to existing two serial axis configuration heliostats, namely the Azimuth-Elevation (Az-EL) and the
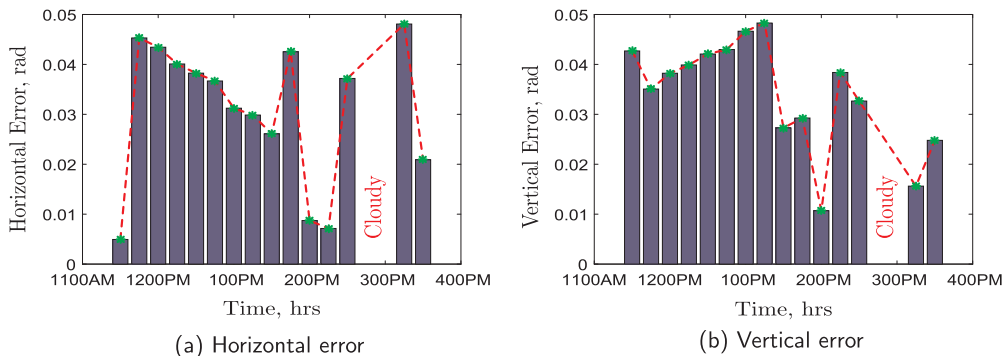
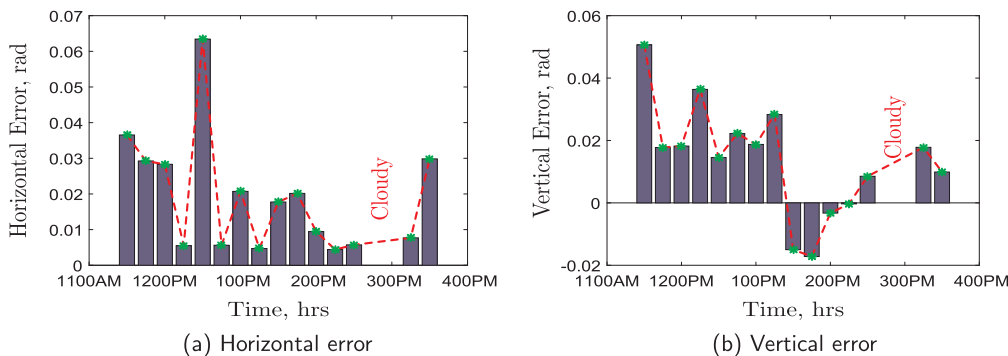**Fig. 18.** Error bar plot of 3-RPS heliostat.

(a) Horizontal error

(b) Vertical error

Fig. 19. Error bar plot of Az-El heliostat.

(a) Horizontal error

(b) Vertical error

Target-Aligned (T-A) configurations. The 3-RPS manipulator significantly reduces the spillage losses when compared to the conventional Az-El and T-A configurations and this has been verified both by
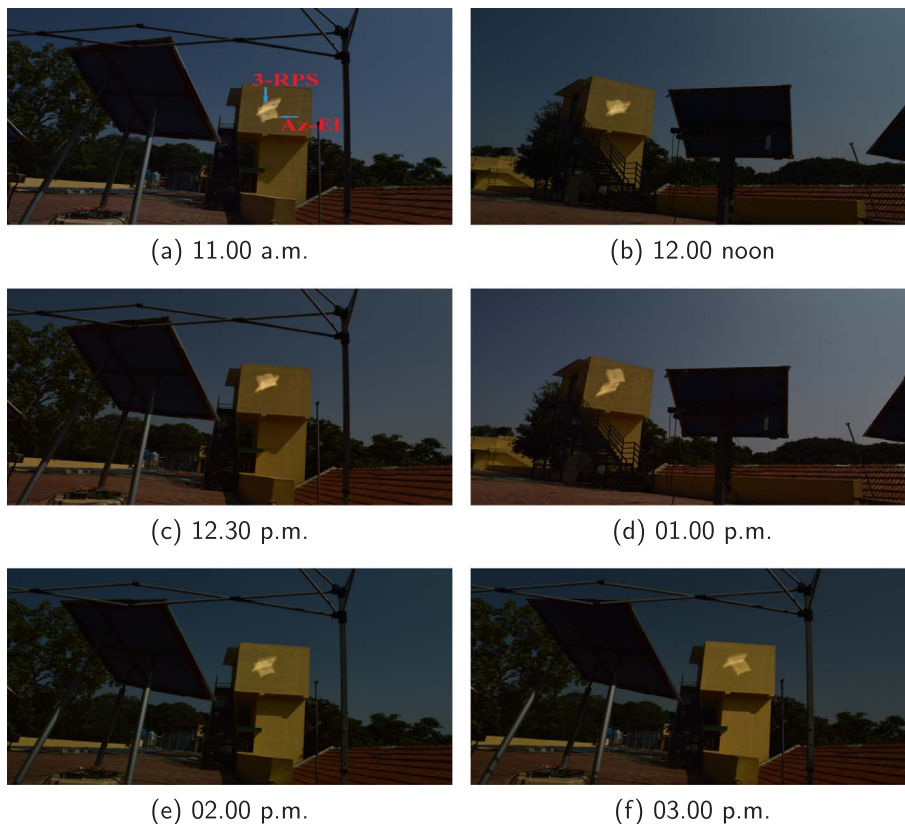
Fig. 21. Deviation of image from the aim-point.

(a) 11.00 a.m.

(b) 12.00 noon

(c) 12.30 p.m.

(d) 01.00 p.m.

(e) 02.00 p.m.

(f) 03.00 p.m.

simulations and experiments. When the heliostat is stationary, the actuators need not be energized to support the weight as the actuators are not back drivable and hence, in the case of the 3-RPS heliostat, energy losses will be less. An iterative search based approach has been presented to find the design parameters of the 3-RPS manipulator which would minimize the actuation required and the spillage losses. A control strategy has been devised in MATLAB-Simulink, implemented on a micro-controller and has been verified for actual sun tracking. It is shown that the 3-RPS configuration is capable of sun tracking with similar errors as the Azimuth-Elevation configuration.

One of the major areas of focus for future works would be to reduce the pointing errors substantially. For this, as mentioned before, a more precise manufacturing methodology has to be adopted and also to find out joints with less play. Additionally, experiments in presence of wind gusts have not been done due to a lack of experimental facilities and this is also an area of future work.

Acknowledgment

References

Altuzarra, O., Macho, E., Aginaga, J., Petuya, V., 2014. Design of a solar tracking parallel mechanism with low energy consumption. Proc. Inst. Mech. Eng. Part C: J. Mech. Eng. Sci 0954406214537249.

Arbes, F., Weinrebe, G., Wöhrbach, M., 2016. Heliostat field cost reduction by slope driveoptimization. In: AIP Conference Proceedings, vol. 1734, AIP Publishing, p. 160002.

Baheti, R., Scott, P., 1980. Design of self-calibrating controllers for heliostats in a solar power plant. IEEE Trans. Autom. Contr. 25 (6), 1091–1097.

Balz, M., Göcke, V., Keck, T., von Reeken, F., Weinrebe, G., Wöhrbach, M., 2016. Stellio–development, construction and testing of a smart heliostat. In: AIP Conference Proceedings, vol. 1734, AIP Publishing, p. 020002.

Berenguel, M., Rubio, F., Valverde, A., Lara, P., Arahal, M., Camacho, E., López, M., 2004. An artificial vision-based control system for automatic heliostat positioning offset correction in a central receiver solar power plant. Sol. Energy 76 (5), 563–575.

Cammarata, A., 2015. Optimized design of a large-workspace 2-dof parallel robot for solar tracking systems. Mech. Mach. Theory 83, 175–186.

Carricato, M., Parenti-Castelli, V., 2004. A novel fully decoupled two-degrees-of-freedom parallel wrist. Int. J. Robot. Res. 23 (6), 661–667.

Chen, Y., Chong, K., Bligh, T., Chen, L., Yunus, J., Kannan, K., Lim, B., Lim, C., Alias, M., Bidin, N., 2001. Non-imaging, focusing heliostat. Sol. Energy 71 (3), 155–164.

Chen, Y., Kribus, A., Lim, B., Lim, C., Chong, K., Karni, J., Buck, R., Pfahl, A., Bligh, T., 2004. Comparison of two sun tracking methods in the application of a heliostat field. J. Sol. Energy Eng. 126 (1), 638–644.

Delgado, F.J., Quero, J.M., Garcia, J., Tarrida, C.L., Ortega, P.R., Bermejo, S., 2012. Accurate and wide-field-of-view mems-based sun sensor for industrial applications. IEEE Trans. Ind. Electron. 59 (12), 4871–4880.

Dunlop, G., Jones, T., 1999. Position analysis of a two dof parallel mechanism the Canterbury tracker. Mech. Mach. Theory 34 (4), 599–614.

Freeman, J., Shankar, B., Sundaram, G., 2017. Inverse kinematics of a dual linear actuator pitch/roll heliostat. In: AIP Conference Proceedings, vol. 1850, AIP Publishing, p. 030018.

Ghosal, A., 2006. Robotics Fundamental Concepts and Analysis. Oxford University Press, New Delhi, India.

Google Inc., 2017. Heliostat Cable Actuation System Design. < https://www.google.org/pdfs/google_heliostat_cable_actuation.pdf > (last accessed August 5, 2017).

Google Inc., 2017. Heliostat Optical Simulation Tool (Hops). < https://code.google.com/p/hops/ > (last accessed August 5, 2017).

Gosselin, C.M., Caron, F., October 19 1999. Two Degree-of-freedom Spherical Orienting Device. US Patent 5,966,991.

Guo, M., Wang, Z., Liang, W., Zhang, X., Zang, C., Lu, Z., Wei, X., 2010. Tracking formulas and strategies for a receiver oriented dual-axis tracking toroidal heliostat. Sol. Energy 84 (6), 939–947.

Igel, E.A., Hughes, R.L., 1979. Optical analysis of solar facility heliostats. Sol. Energy 22 (3), 283–295.

Jones, S.A., Stone, K., 1999. Analysis of Solar Two Heliostat Tracking Error Sources. Technical Report, Sandia National Laboratories, Albuquerque, NM, and Livermore, CA.

King, D., Arvizu, D., 1981. Heliostat characterization at the central receiver test facility. J. Sol.Energy Eng. 103 (2), 82–88.

Kribus, A., Vishnevetsky, I., Yogev, A., Rubinov, T., 2004. Closed loop control of heliostats. Energy 29 (5), 905–913.

Lee, K.-M., Shah, D.K., 1988. Kinematic analysis of a three-degrees-of-freedom in-parallel actuated manipulator. IEEE J. Robot. Automat. 4 (3), 354–360.

Lee, C.-Y., Chou, P.-C., Chiang, C.-M., Lin, C.-F., 2009. Sun tracking systems: a review. Sensors 9 (5), 3875–3890.

Li, W., Sun, J., Zhang, J., He, K., Du, R., 2006. A novel parallel 2-dof spherical mechanism with one-to-one input-output mapping. WSEAS Trans. Syst. 5 (6), 1343–1348.

Lindberg, V., Maki, J.-P., 2010. SKF Dual Axis Solar Tracker-from Concept to Product, Chalmers University, Sweden.

Lipps, F., Vant-Hull, L., 1978. A cellwise method for the optimization of large central receiver systems. Sol. Energy 20 (6), 505–516.

MATLAB, 2012. Natick, Massachusetts.

Mendelsohn, M., Lowder, T., Canavan, B., 2012. Utility-scale Concentrating Solar Power and Photovoltaics Projects: A Technology and Market Overview. NREL Technical Report, NREL/TP-6A20-51137 303, pp. 275–3000.

Mousazadeh, H., Keyhani, A., Javadi, A., Mobli, H., Abrinia, K., Sharifi, A., 2009. A review of principle and sun-tracking methods for maximizing solar systems output. Renew. Sustain. Energy Rev. 13 (8), 1800–1818.

NREL, 2017. National Renewable Energy Labarotary. < http://www.nrel.gov/csp/solarpaces/project_detail.cfm/projectID=62 > (last accessed August 5, 2017).

Quero, J.M., Aracil, C., Franquelo, L.G., Ricart, J., Ortega, P.R., Domínguez, M., Castañer, L.M., Osuna, R., 2007. Tracking control system using an incident radiation angle microsensor. IEEE Trans. Ind. Electron. 54 (2), 1207–1216.

Reda, I., Andreas, A., 2004. Solar position algorithm for solar radiation applications. Sol. Energy 76 (5), 577–589.

Ries, H., Schubnell, M., 1990. The optics of a two-stage solar furnace. Sol. Energy Mater. 21 (2), 213–217.

Roman, E., Alonso, R., Ibañez, P., Elorduizapatarietxe, S., Goitia, D., 2006. Intelligent PV module for grid-connected PV systems. IEEE Trans. Ind. Electron. 53 (4), 1066–1073.

Ruggiu, M., 2010. Kinematic and dynamic analysis of a two-degree-of-freedom spherical wrist. J. Mech. Robot. 2 (3), 031006.

Shyam, R.A., Ghosal, A., 2015. Three-degree-of-freedom parallel manipulator to track the sun for concentrated solar power systems. Chin. J. Mech. Eng. 28 (4), 793–800.

Srivatsan, R.A., Bandyopadhyay, S., Ghosal, A., 2013. Analysis of the degrees-of-freedom of spatial parallel manipulators in regular and singular configurations. Mech. Mach. Theory 69, 127–141.

Stine, W.B., Geyer, M., 2001. Power from the Sun, Power from the sun.net.

Vant-Hull, L., 2012. Concentrating Solar Power Technology: Principles, Developments and Applications. Woodhead Publishing, Cambridge, UK (Chapter 8).

Wei, X., Lu, Z., Yu, W., Zhang, H., Wang, Z., 2011. Tracking and ray tracing equations for the target-aligned heliostat for solar tower power plants. Renew. Energy 36 (10), 2687–2693.

Zaibel, R., Dagan, E., Karni, J., Ries, H., 1995. An astigmatic corrected target-aligned heliostat for high concentration. Sol. Energy Mater. Sol. Cells 37 (2), 191–202.